Computational Study of Film Cooling Effectiveness for a Comparison of Cylindrical, Square and Triangular Holes of Equal Cross-Sectional Area

FAYYAZ HASSAN ASGHAR*, AND MUHAMMAD JAVED HYDER*

RECEIVED ON 10.11.2008 ACCEPTED ON 04.03.2009

ABSTRACT

Film cooling effectiveness is studied computationally for a comparison of circular, square and two types of equilateral triangular holes with an inclination of 30° with streamwise direction. Reynolds number based on the freestream velocity and hole diameter is 10364. Length to diameter ratio of circular hole is 4, which is representative of gas turbine engines. The coolant to mainstream density ratio is 0.92. Main flow is supplied at the temperature of 293.15K and coolant is supplied at 318.15K. Centerline and laterally averaged effectiveness are presented for film cooling measurements. Current computational results for circular hole are compared with experimental results. Computational results are well in agreement with the experimental results even for high blowing ratios. Blowing ratios ranging from 0.33-2.0 have been investigated. It is observed that triangular hole having lateral straight edge on leeward side shows much higher effectiveness values than circular film cooling hole case in the near hole region and almost similar coolant jet height as that in case of circular film cooling. Also it is observed that triangular hole having lateral straight edge on windward side and converging corner on leeward side shows lesser coolant jet height and higher film cooling effectiveness in the region x/D≥10, especially at blowing ratios greater than 1.0.

Key Words: **CFD, Film Cooling Effectiveness, Heat Transfer, Fluid Flow, Turbine Blade Cooling.**

1. INTRODUCTION

Film cooling is commonly used in modern gas turbine engines to protect hot section components from failure at the elevated temperature of combustion gases. For better turbine efficiency higher turbine inlet temperatures are needed so a thorough understanding of film cooling physics has become crucial to making further advances in cooling technology.

In film cooling, cool air is bled from the compressor stage, ducted to the internal chambers of the turbine blades, and discharged through small holes in the blade walls. This air provides a thin, cool, insulating blanket along the external surface of the turbine blade.

Film cooling is usually measured in dimensionless form known as "film cooling effectiveness", mathematically it is defined as:

* Department of Mechanical Engineering, Pakistan Institute of Engineering and Applied Sciences, Nilore, Islamabad.

$$\eta = \frac{T_{aw} - T_\infty}{T_C - T_\infty} \quad (1)$$

where T_{aw} is adiabatic wall temperature, T_∞ is freestream temperature = 293.15 K, and T_c is coolant inlet temperature = 318.15 K

To study film cooling phenomena, investigators have been using simple geometries to reduce the complexity of the flow affecting the heat exchange between the test surface and the mainstream gas flow. The geometrically simple form of a flat plate (instead of actual turbine blade shape) with one or more film cooling holes often offers a sufficient approximation of the reality for a lot of research interests [1-3].

1.1 Review of Literature

Effectiveness results from a single circular hole and row of holes were reported by [4-5]. Their study reported a blowing ratio (M) of 0.5 for maximum effectiveness at coolant to freestream DR (Density Ratio) around 1.0. However, test flow conditions did not resemble those found in gas turbine engines (density ratio greater than 1.0). Turbine inlet temperatures of up to 1700K and coolant air temperature in the range of 700-1000K are common in modern jet engines [6], resulting in coolant-to-mainstream density ratios well in excess of unity.

Single discrete jet, injected normally and at a 30° angle to the crossflow, were examined by [7-8]. The authors documented jet lift-off and penetration of the crossflow boundary layer as blowing ratio increased, as well as the influence of the crossflow on the flow within the film hole itself. A detailed analysis of an isolated normal jet in crossflow was presented by [9]. The authors found the counter rotating vortex pair downstream of jet injection. Film cooling effectiveness using a circular hole at an angle of 30, 60, and 90° was studied by [10]. A hole length of L=4D was used, the free-stream Reynolds number based on the free-stream velocity and hole diameter was 8563, and the blowing ratio was varied from 0.33-2. For a single 30° hole, in the region immediately downstream of the hole the maximum effectiveness occurred for a blowing ratio less than 0.5. Downstream of this immediate region, centerline effectiveness and lateral spread increased up to a blowing ratio of 0.5, then decreased with increasing blowing ratio due to jet penetration into the free stream. Also, the region with effectiveness greater than 0.2 did not extend beyond x/D=13. Film Effectiveness and heat transfer coefficients for a rows of round holes with different hole inclinations were investigated by [11-12]. Flow structure for flat plate film cooling for different blowing ratios was investigated by [13]. They found decrease of boundary layer thickness with increasing blowing ratio and they proposed that increase in heat transfer coefficient with increasing blowing ratio is associated with this decrease of boundary layer thickness.

Mean velocities and turbulent kinetic energy fields for lateral jet in Crossflow at inject angle of -60 degree and -30 degree were numerically investigated by [14]. They employed RNG k-e turbulence model with two layer wall function method. They found separation events in the lee of the jet exit and behind the jet. Commercial software FLUENT was used by [15] to study the effect of injecting a small amount of water into the cooling air for film cooling performance. They did the computations at gas turbine operating conditions, at a pressure of 15 atmospheric and a temperature of 1561K. They found that 10-20% mist achieved 5-10% cooling effectiveness. Effect of hole imperfection on adiabatic film cooling effectiveness was investigated by [16]. Half torus inside the cooling hole is used as a discrete imperfection. Film cooling effectiveness was found with the presence of imperfection at different positions. It was founded that the imperfection placed one diameter from the hole leading edge deteriorated the effectiveness at moderate velocity ratios while the same imperfection fixed at the hole exit improved the effectiveness. Influence of different hole shapes on film cooling with CO_2 injection was investigated by [17]. Hole shapes investigated include

cylindrical holes, 3-in-1 holes and fanned holes. In terms of film cooling performance, the fanned holes were found best while the cylindrical holes were found worst among the three hole shapes tested.

Aim and objective of present work is to computationally study the behavior of new hole shapes for film cooling effectiveness and to predict that which hole shapes provide better cooling effectiveness.

2. METHODOLOGY

In the first part of present study, the benchmark experimental study of [10] is used as a test case to compare the results of circular cooling hole. They studied film cooling through single circular hole having streamwise (x-direction) inclination of 30, 60 and 90°. A schematic of the geometrical model (with dimensions in millimeters) for the circular-hole case used for CFD simulations is shown in Fig. 1.The exact dimensions and parameters have been chosen so that the results can be compared to those discussed in [10].

In the second part of present study, square and triangular hole shapes have been investigated. Cross-sectional area of all hole shapes used in this work is kept same as that of circular hole. For triangular hole shapes, two types of equilateral triangular holes have been investigated. First has one corner at the windward side and straight edge at the leeward side this hole will be called triangular hole-1 in the following text, while second has straight edge at windward side and corner at leeward side and this hole will be called as triangular hole-2 in the following text. Fig. 2 shows the cross-section of all hole shapes used.

2.1 Boundary Conditions

At all boundaries except those denoted as "main inlet," "coolant inlet," "outlet" in Fig. 1, and symmetry

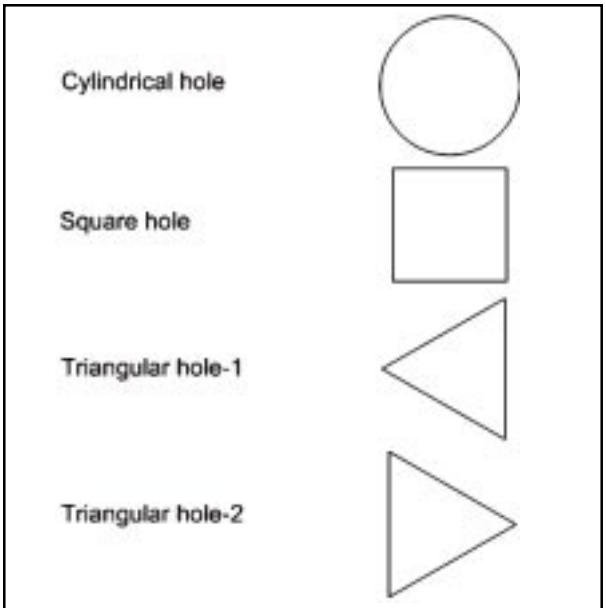

FIG. 2. HOLE SHAPES

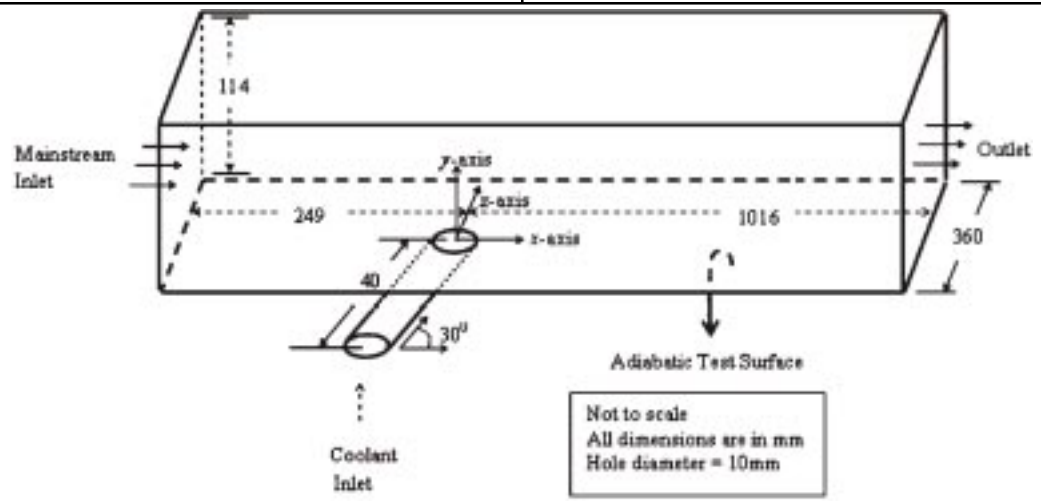

FIG. 1 GEOMETRY OF TEST CASE FOR CFD SIMULATION

boundary conditions (not shown in Fig. 1), an adiabatic wall boundary condition is used. At the "main inlet," a velocity-inlet boundary condition is specified with x-velocity equal to 13 m/s and all other components equal to zero. The temperature is given as 293.15K at the main inlet. The turbulence intensity and hydraulic diameter (which is used to determine turbulence length scales) are specified as 2.7% and 139.59mm, respectively. At the "coolant inlet", a velocity-inlet boundary condition is varied case to case and detail of velocity inlet conditions is specified in Table 1 and the inlet temperature of the coolant is 318.15K to match the coolant to freestream density ratio of 0.92 with experiment of [10]. The turbulence intensity and hydraulic diameter are specified as 3% and 10mm, respectively. At the "outlet", a pressure-outlet boundary condition is specified with gage pressure equal to 0 (giving an absolute pressure of 101,325 Pa).

Cooling hole inlet velocities (V_c) are calculated as

$$V_c = 13(\text{m/sec}) \times VR \quad (2)$$

$$\text{Where} \quad VR = \frac{M}{DR} \quad (3)$$

The geometry consists of a single hole streamwise inclined at an angle of 30^0. Cylindrical hole length to diameter ratio is 4. Reynolds number based on freestream velocity and hole diameter is 10364. Blowing ratios ranging from 0.33-2 have been investigated.

TABLE 1. PLENUM INLET VELOCITIES

Case No.	Blowing Ratio (M)	VR	V_c (m/sec)
1.	0.33	0.358	4.654
2.	0.50	0.543	7.059
3.	0.67	0.727	9.451
4.	1.00	1.086	14.118
5.	1.33	1.444	18.772
6.	1.67	1.813	23.569
7.	2.0	2.171	28.223

2.2 Grid Independency

For grid independent study, the circular hole case for blowing ratio of M=0.33 and hole streamwise inclination 30^o is selected. Different meshes have been tried. Fig. 3 shows the mesh independency for centerline effectiveness. Table 2 shows the grid sizes for different meshes. By observing the Fig. 3, it is clear that the result in case of medium and fine meshes almost similar. Hence medium mesh is used for analysis.

2.3 Solver

A 3D segregated, steady state solver is used. For linearization of governing equations implicit method is used. For turbulence modeling k-ε model [18] with standard wall functions [19] is used. To avoid use of enhanced wall treatment mesh was kept fine enough to have wall Y+ in the range 0-5.

Discretization scheme used is 2nd order upwind [20] for momentum, turbulence kinetic energy, turbulence dissipation rate and energy, whereas for pressure standard

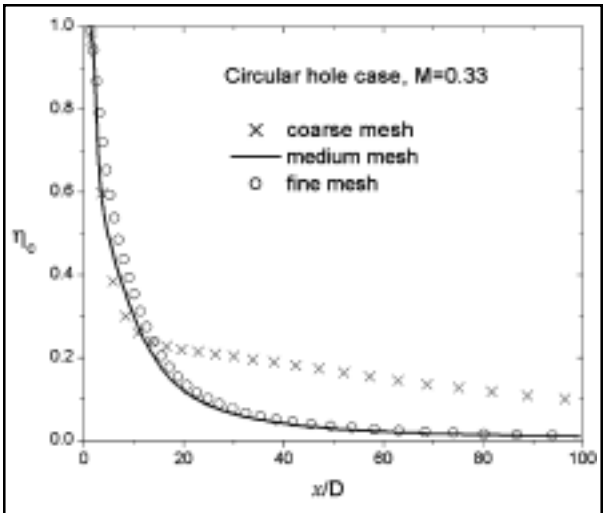

FIG. 3. MESH INDEPENDENCY

TABLE 2. GRID SIZES FOR DIFFERENT MESHES

Grid Size	Coarse	Medium	Fine
Cells	241773	1270773	1914773
Faces	732551	3850718	5797736
Nodes	246849	1301289	1955529

discretization scheme [21] is used. For pressure-velocity coupling SIMPLE algorithm [22] is used.

2.4 Governing Equations

The steady state continuity and momentum equations in indicial notation are:

$$\frac{\partial u_i}{\partial x_i} = 0 \tag{4}$$

and

$$\frac{\partial}{\partial x_j}(\rho u_i u_j) = -\frac{\partial p}{\partial x_j} + \frac{\partial}{\partial x_j}\left[\mu\left(\frac{\partial u_i}{\partial x_j} + \frac{\partial u_j}{\partial x_i} - \frac{2}{3}\delta_{ij}\frac{\partial u_l}{\partial x_l}\right)\right] + \frac{\partial}{\partial x_j}\left(-\rho\overline{u_i' u_j'}\right) \tag{5}$$

where

$$-\rho\overline{u_i' u_j'} = \mu_t\left(\frac{\partial u_i}{\partial x_j} + \frac{\partial u_j}{\partial x_i}\right) - \frac{2}{3}\left(\rho k + \mu_t\frac{\partial u_i}{\partial x_i}\right)\delta_{ij} \tag{6}$$

Two additional transport equations (for the turbulence kinetic energy, k, and the turbulence dissipation rate, ε, are solved, and Turbulent viscosity (μ_t) is computed as a function of k and ε.

$$\rho\frac{\partial}{\partial x_i}(k u_i) = \frac{\partial}{\partial x_j}\left[\left(\mu + \frac{\mu_t}{\sigma_k}\right)\frac{\partial k}{\partial x_j}\right] + G_k - \rho\varepsilon \tag{7}$$

$$\rho\frac{\partial}{\partial x_i}(\varepsilon u_i) = \frac{\partial}{\partial x_j}\left[\left(\mu + \frac{\mu_t}{\sigma_\varepsilon}\right)\frac{\partial \varepsilon}{\partial x_j}\right] + C_{1\varepsilon}\frac{\varepsilon}{k}G_k - C_{2\varepsilon}\rho\frac{\varepsilon^2}{k} \tag{8}$$

$$\mu_t = \rho C_\mu \frac{k^2}{\varepsilon} \tag{9}$$

The generation of turbulence kinetic energy (G_k) is calculated using:

$$G_k = -\rho\overline{u_i' u_j'}\frac{\partial u_j}{\partial x_i} \tag{10}$$

where as the model constant $C_{1\varepsilon}$, $C_{2\varepsilon}$ and C_μ are taken as the default values ($C_{1\varepsilon}$=1.44, $C_{2\varepsilon}$=1.92 and C_μ=0.09) in FLUENT.

Also the model constants known as the turbulent Prandtl number for k is taken as σ_k=1.0 and the model constant known as turbulent Prandtl number for ε is used as σ_ε=1.3.

As these modal constant values are standard one and have been found to work fairly well with wide range of wall bounded and free shear flows, hence the same are used for the present computational model.

The energy equation for the present problem is described as:

$$\frac{\partial}{\partial x_i}\left[u_i(\rho E + p)\right] = \frac{\partial}{\partial x_j}\left[k_{eff}\frac{\partial T}{\partial x_j}\right] \tag{11}$$

where E is the total energy and k_{eff} is the effective thermal conductivity, given by:

$$k_{eff} = k + \frac{c_p u_t}{\mathrm{Pr}_t} \tag{12}$$

3 RESULTS AND DISCUSSION

The performance of film cooling scheme is given in terms of centerline and laterally averaged adiabatic effectiveness. For validation purpose CFD results for baseline case of circular hole are compared with experimental results of [10]. Results shown in Fig.4 for centerline film cooling effectiveness and in Fig.5 for laterally averaged film cooling effectiveness reveal that the centerline effectiveness is very much in agreement with the experimental results (Fig. 4) in the entire region except in the near hole region (x/D≤5.0). Immediate decrease of centerline effectiveness is due to either the mainstream penetration in to coolant jet or due to coolant jet lift-off from the adiabatic test surface, For low blowing ratios of M=0.33, 0.50 as the coolant velocities

are smaller as compare to mainstream velocity so jet lift-off is low as clear from higher centerline effectiveness in the near hole region, the immediate decrease of effectiveness for these low blowing ratios in near hole region is due to the penetration of mainstream fluid into the coolant jet. For blowing ratios greater than 0.5, η_c decreases to very low values in the near hole region, this is due to the jet lifting-off from the surface. Computational results for laterally averaged effectiveness $\bar{\eta}$ are in excellent agreement with experimental results of [10] for the blowing ratios of M=0.67-2.0 (Fig. 5(c-f). However, for low blowing ratios of M=0.33, 0.50 (Fig.5 (a-b)), CFD results show slight over prediction of than that seen in experiment [10]. It is seen that for low blowing ratios of M=0.33 and 0.50, η values are higher than that from blowing ratios greater than 0.5, reason is the more spread of coolant at lower blowing ratios due to the mainstream fluid penetration with in the coolant jet. Usually in literature computational results are not found to be well in agreement with experimental results for higher blowing ratios. But present computational results are in excellent agreement with experimental results for high blowing ratios. This is due to the choice of a good grid after grid independent study and also due to the absence of coolant plenum which is avoided here in this work to correctly apply the blowing ratio at coolant hole inlet. Coolant jet lift-off from test surface (shown by immediate decrease of effectiveness) is excellently predicted, also for a blowing ratio M=1.0,

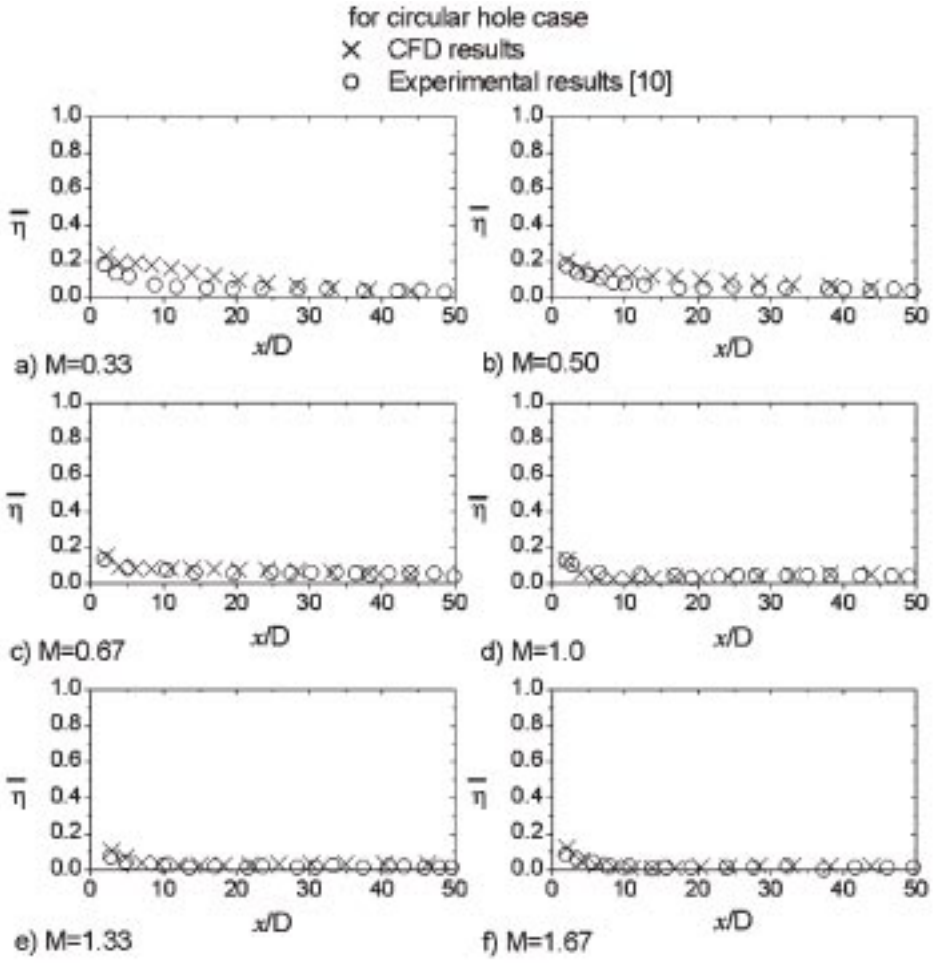

FIG. 4. COMPARISON OF CFD RESULTS OF η_c WITH EXPERIMENT

after coolant jet lift-off, a little reattachment of the coolant jet with the test surface (shown by increase in effectiveness) is also predicted in computational results of laterally averaged effectiveness (Fig. 5(d)), as seen in experimental results of [10].

Comparison of centerline (z/D=0.0) adiabatic film cooling effectiveness (η_c) for different types of film cooling hole shapes (circular, square, triangle hole-1 and triangle hole-2) is shown in Fig. 6. For the low blowing ratio of 0.33, η_c for all film cooling hole shapes is seen to reduce slowly (Fig. 6(a)) along streamwise direction as compare to blowing ratio higher than 0.33 (Fig. 6(b-d)) showing less lift-off of coolant jet at blowing ratio of 0.33. Among all the film cooling holes studied, η_c for triangular hole-1 case is much higher in the near hole region (up to x/D=15), after x/D≥15 triangular hole-1 case shows similar values of η_c as circular hole case. Triangular hole-2 shows higher η_c than circular hole case at M=0.33, 0.67 and 1.0 (Fig. 6(a-c)). For the blowing ratios of M=1.33-2.0, triangular hole-2 case show almost similar or little lower centerline effectiveness than that of circular hole in the region x/D=10. But in the region x/D≥10, and for blowing ratios M=1.33-2.0, triangular hole-2 case shows higher η_c than other hole shapes due to the reattachment of coolant jet with the test surface, this reattachment of coolant is more pronounced at blowing ratio of 2.0.

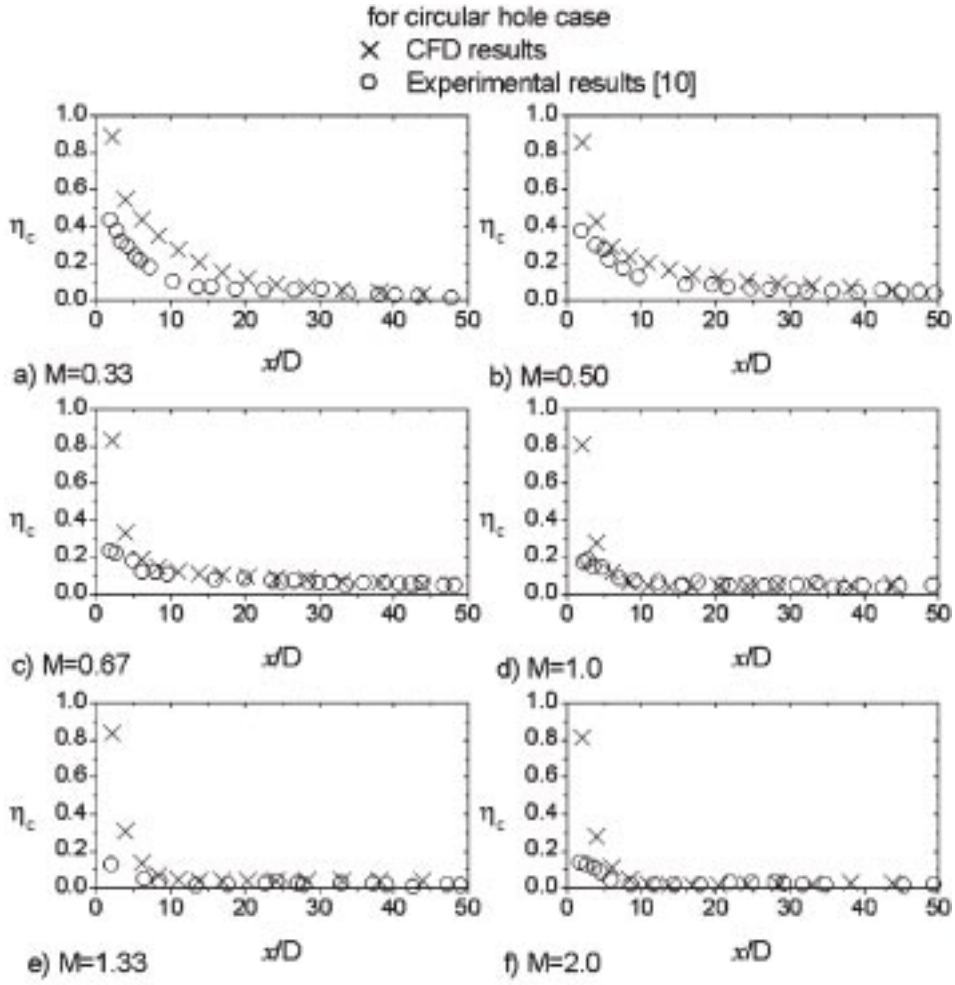

FIG. 5. COMPARISON OF CFD RESULTS OF $\overline{\eta}$ WITH EXPERIMENT

Fig. 7 shows the comparison of laterally averaged effectiveness for different hole shapes and blowing ratios. Here again as seen in centerline film cooling effectiveness, the triangular hole-2 shows much higher laterally averaged effectiveness than other hole shapes in the near hole region ($x/D \leq 10$), however for the region $x/D \geq 10$, triangular hole-1 shows higher effectiveness especially for blowing ratio range M=1.0-2.0 (Fig.7(d-g)), where after early lift-off of coolant jet, reattachment is prominent as can be seen by increased laterally averaged effectiveness.

Fig. 8 shows the average centerline effectiveness , averaged over different streamwise regions. It is seen (Fig. 8(a)) that triangular hole-1 shows highest values of average centerline effectiveness over the region $1 \leq x/D \leq 10$, over all blowing ratios except at M=0.33, where averaged centerline effectiveness for triangular hole-1 is little less than that for triangular hole-2 case. Over the regions $10 \leq x/D \leq 20$ and $20 \leq x/D \leq 50$, η_c is seen to be higher in triangular hole-2 case at almost all blowing ratios (Fig. 8(b-c)). Over the regions $1 \leq x/D \leq 50$ η_c is seen to be higher in triangular hole-1 case at almost all blowing ratios (Fig. 8(d)).

Fig. 9 shows the variation of overall averaged (two dimensionally averaged) effectiveness with different blowing ratios. In two dimensional averages, lateral

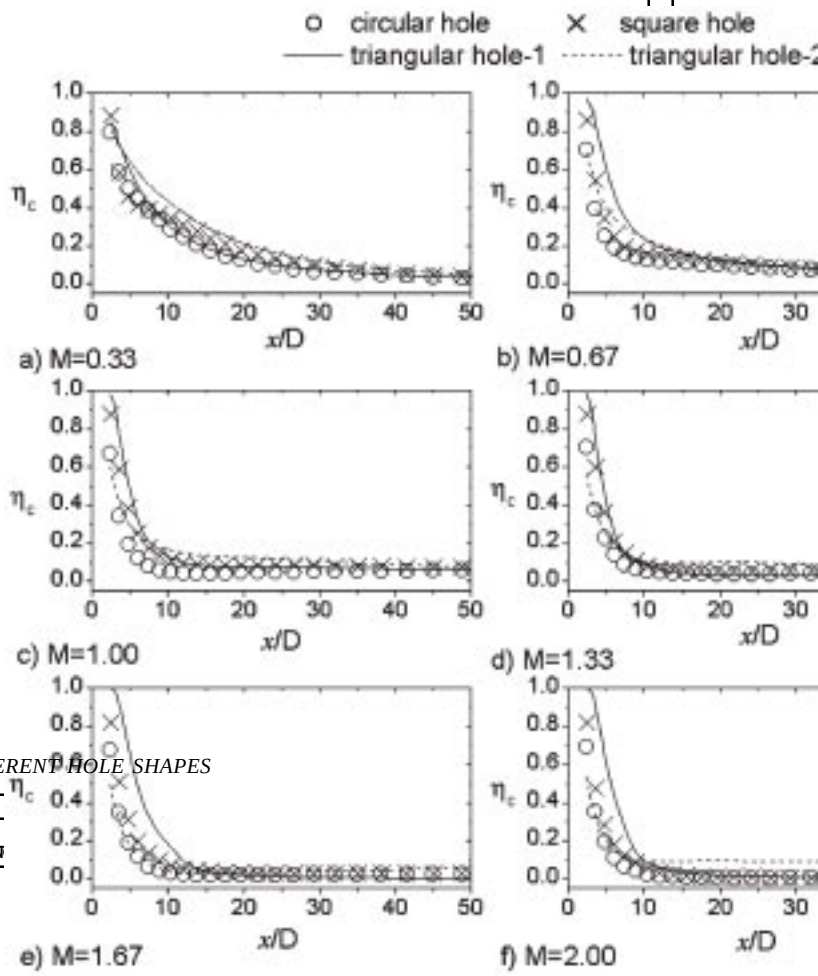

FIG. 6. η_c FOR DIFFERENT HOLE SHAPES

average is taken over the region $0 \leq z/D \leq 1.5$, whereas the streamwise average is taken over different streamwise regions ($1 \leq x/D \leq 10$, $10 \leq x/D \leq 20$, $20 \leq x/D \leq 50$ and $1 \leq x/D \leq 50$). Here again triangular hole-1 shows much higher overall effectiveness over the streamwise region $1 \leq x/D \leq 10$, showing much higher lateral distribution of coolant in that region. While in the regions $10 \leq x/D \leq 20$ and $20 \leq x/D \leq 50$, triangular hole-2 gives higher effectiveness than other film cooling holes. When average is taken over the streamwise region $1 \leq x/D \leq 50$, then both triangular hole shapes shows almost similar overall effectiveness at most of the blowing ratio.

Fig. 10 shows the lateral distribution of effectiveness at x/D=5.2 for different blowing ratios. At this point lateral distribution of effectiveness is much higher for triangular hole-1 as compare to other hole shapes. Also it is seen that lateral distribution of coolant decreases with increasing blowing ratios. Fig. 11 shows the lateral distribution of effectiveness at x/D=15 for different blowing ratios. At this point lateral distribution of effectiveness is much higher for triangular hole-2 as compare to other hole shapes at all blowing ratios. The reason is the more spread of coolant in that region (at x/D=15) in case of triangular hole-2 as compare to other hole shapes.

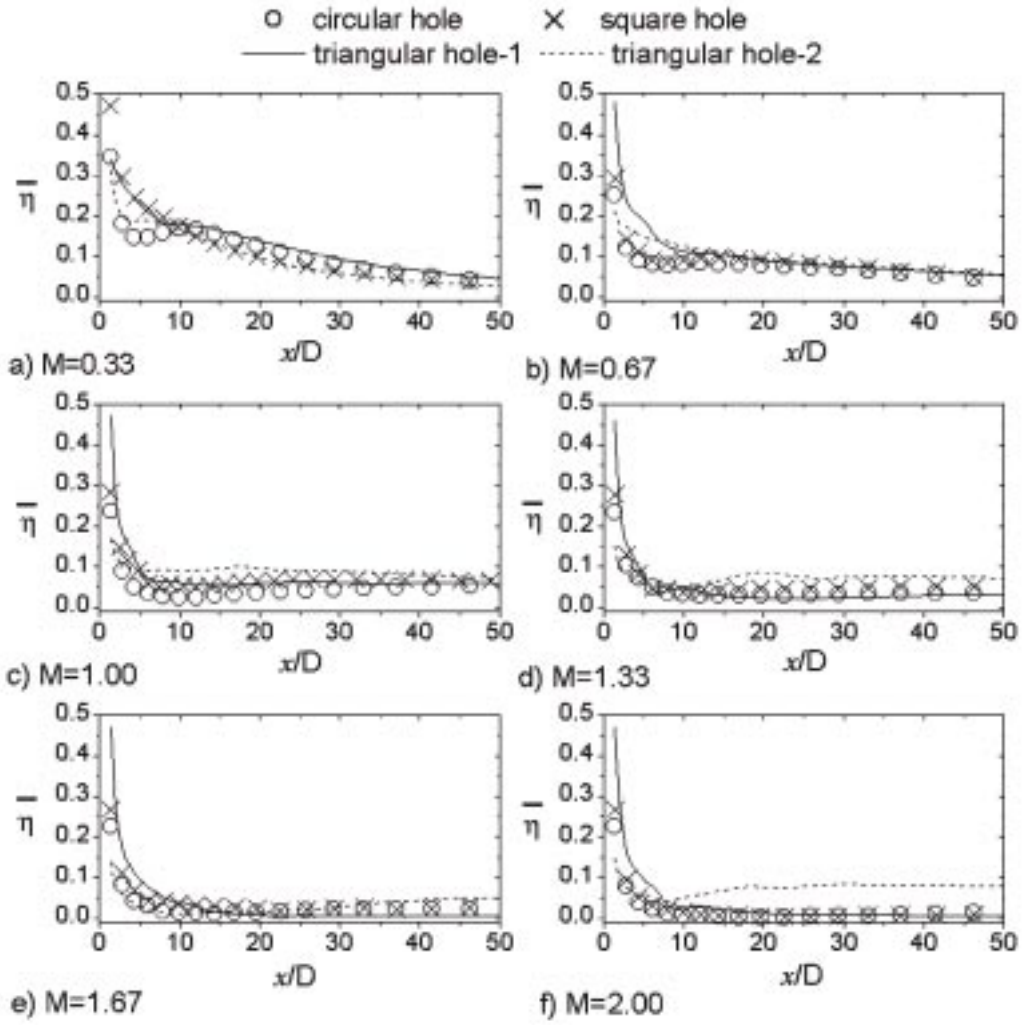

FIG. 7. $\bar{\eta}$ FOR DIFFERENT HOLE SHAPES AT DIFFERENT BLOWING RATIOS

For the film cooling of turbine blade, along with higher effectiveness it is also required coolant jet penetrate less in to the main fluid. For this coolant jet height is calculated at z/D=0.0 and at different streamwise location. As main fluid temperature was 293.15K and that of coolant was 318.15K. Coolant jet height is measured by the temperature profiles of fluid. The height at which temperature reaches the 293.15K (temperature of main fluid) and there is no further change in temperature showing no presence of coolant above that height will be called here as coolant jet height. Fig. 12 shows the temperature profiles at x/D=5.2 and z/D=0.0 for different blowing ratios. The coolant jet height at x/D=5.2 for triangular hole-1 is same as the coolant jet height of circular case. However, coolant jet height of triangular hole-2 is smaller than the other cases at blowing ratios of M=1.33-2.0 (Fig. 12 (d-f)). In the region near the test plate (e.g. in the region $0 \leq y/D \leq 0.5$), the lower temperature shows more penetration of main fluid (temperature=293.15K) into the coolant (temperature=318.15K), and for all blowing ratios it is seen that both triangular film cooling holes shows less penetration of main fluid of main fluid within the coolant jet, which is the main reason for higher effectiveness in triangular hole cases. Fig. 13 shows the temperature profiles at x/D=20.4 and z/D=0 for different blowing ratios. It is seen that the coolant jet height for all shapes is almost same for blowing ratios of 0.33-1.0. But at

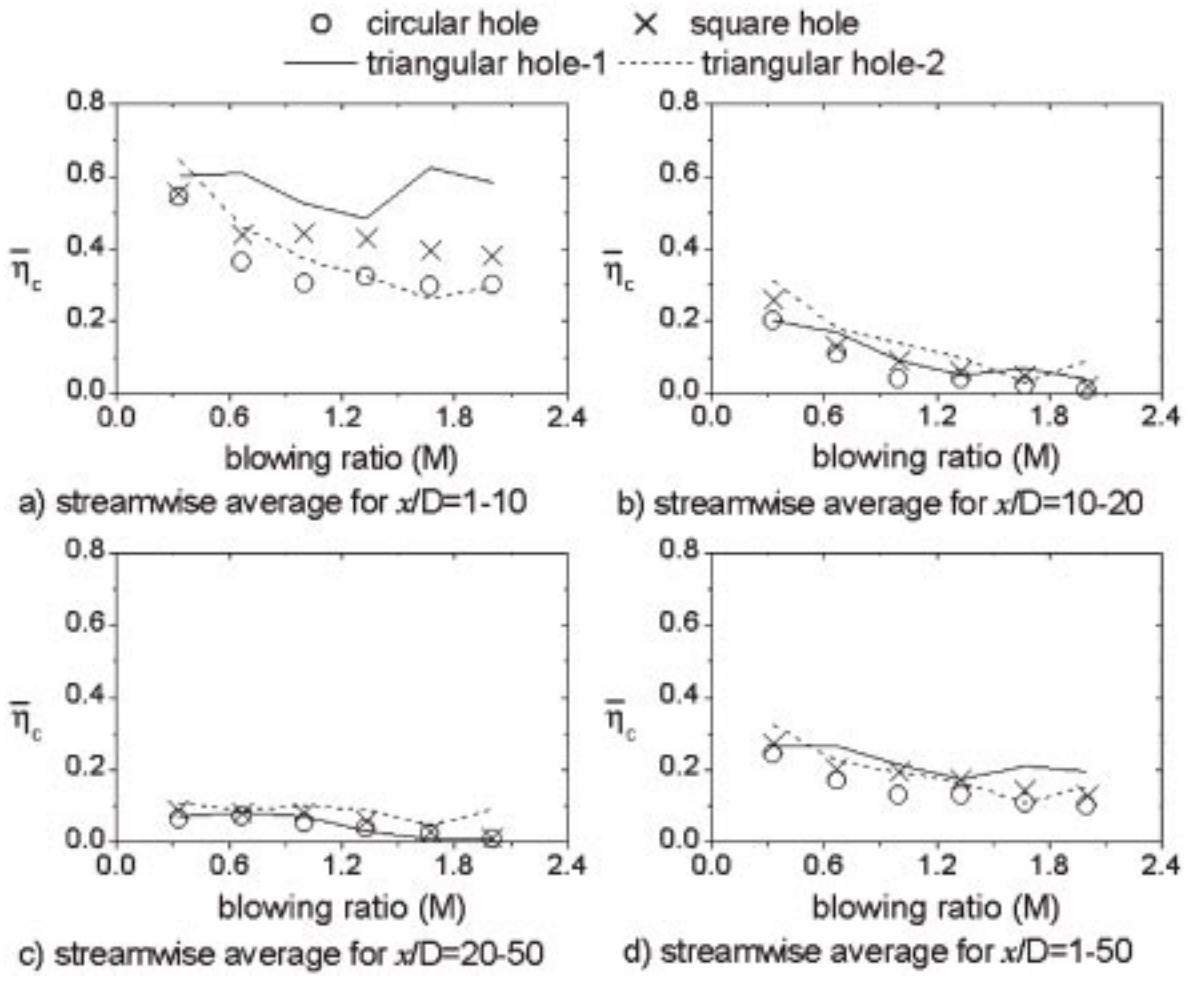

FIG. 8. VARIATION OF $\overline{\eta}_C$ WITH BLOWING RATIOS

higher blowing ratios of M=1.33-20, coolant jet height for triangular hole-2 case is much lower than that of circular hole case. Also in the region near the test plate triangular hole-2 case shows less entrainment of main fluid into the coolant than that of other hole shapes, which is the main reason for higher effectiveness from triangular hole-2 case in that region.

4. CONCLUSIONS

(i) Benchmark experimental work for circular film cooling hole case is successfully modeled with results showing good agreement with the experimental work.

(ii) Among the four different hole shapes studied for film cooling adiabatic effectiveness, the equilateral triangular hole-1 (having same cross-sectional area as that of circular hole and windward side with converging corner) is found to give highest effectiveness in the near hole region $1 \leq x/D \leq 10$, while at a point x/D=5.2 and z/D=0.0 coolant jet height from triangular hole-1 is same as that from circular hole case.

(iii) In the streamwise region $x/D \geq 10$ triangular hole-2 not only found to give highest effectiveness but at high blowing ratios M=1.33-2.0, the coolant jet height is also found to be much less than that of circular hole case.

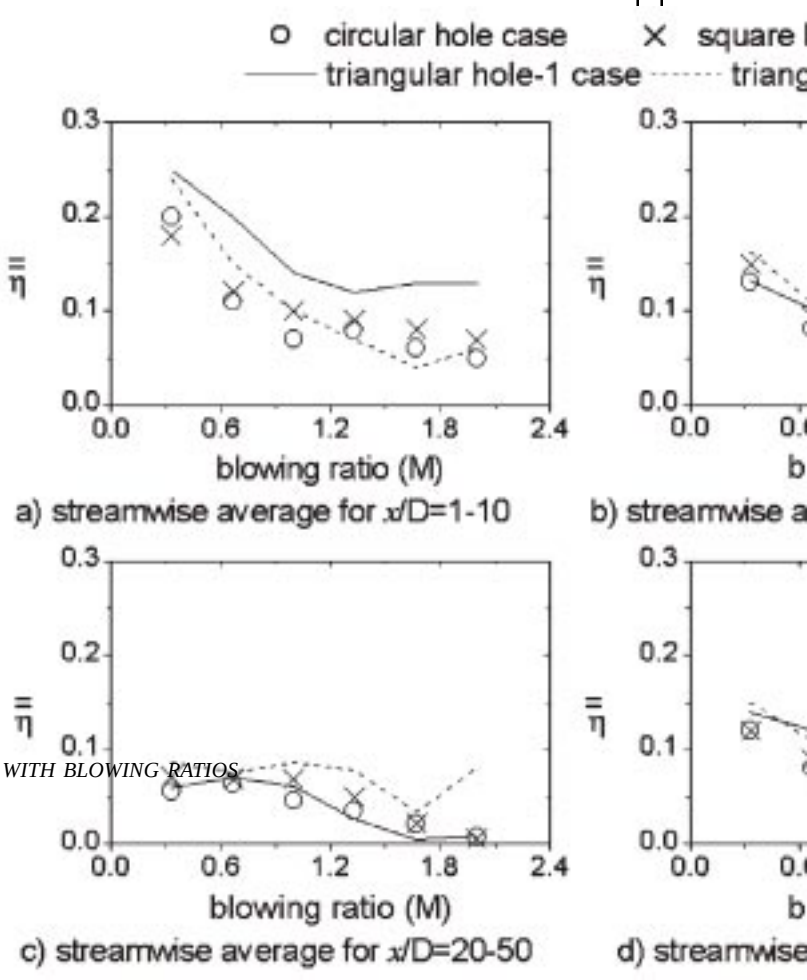

FIG. 9. VARIATION OF $\bar{\eta}$ *WITH BLOWING RATIOS*

(iv) It is also concluded that more lateral width of the cooling hole on the windward side (as in the case of triangular hole-2 case), the coolant jet lift-off is less and also more reattachment of the coolant with the test plate after the near hole region.

(v) It is also concluded that more lateral width at leeward side of film cooling hole as was in the case of triangular hole-1 case, there is less chance of main fluid entrance into the region just downstream of cooling hole thus resulting in higher effectiveness in the region x/D≤10.

Finally authors propose to use triangular film cooling holes instead of circular holes depending upon the region of interest in the streamwise direction.

5. UNITS

Velocity	meter per second (m/s)
Temperature	kelvin (K)
Length	millimeters (mm)
Angle	degree (°)
Pressure	atmospheric (atm)

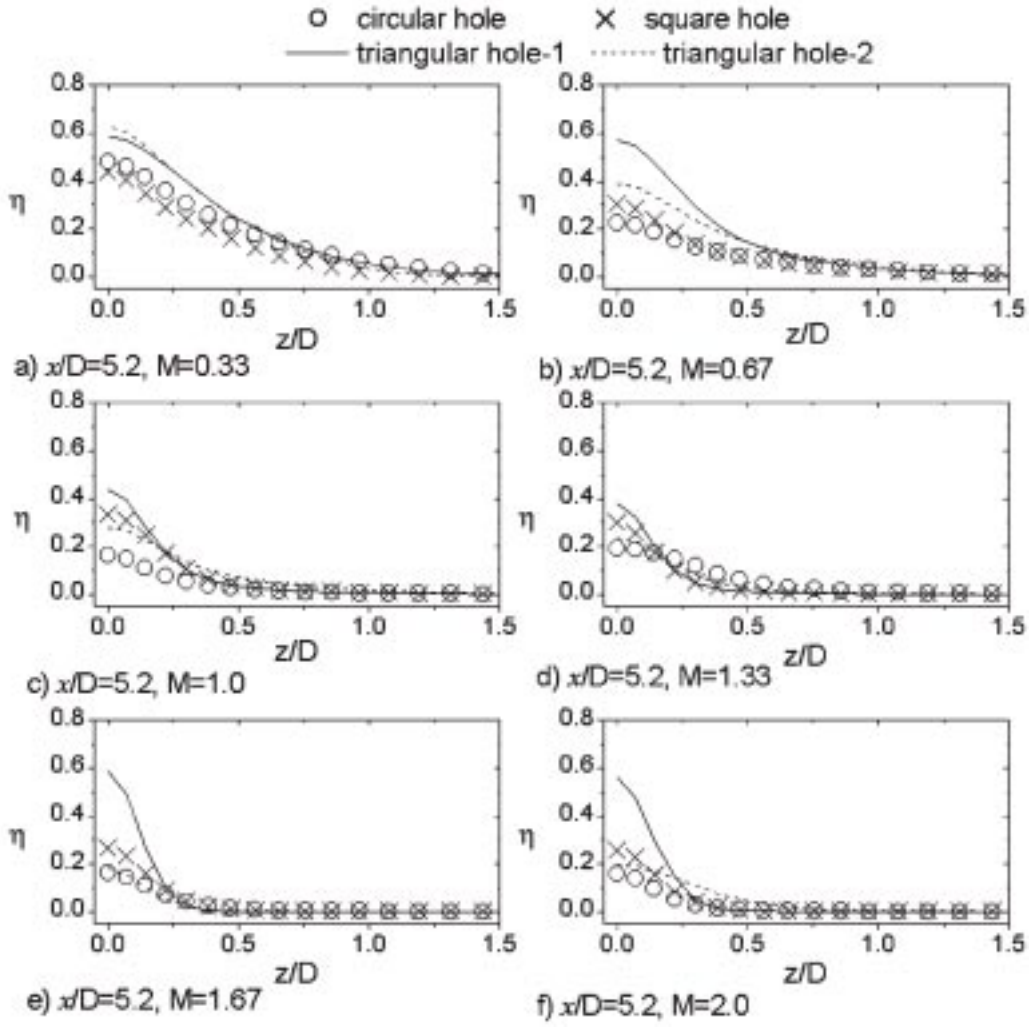

FIG. 10. LATERAL DISTRIBUTION OF EFFECTIVENESS AT X/D=5.2

6. ABBREVIATIONS

DR	Coolant to freestream density ratio
VR	Coolant to freestream velocity ratio
M	Coolant-to-freestream blowing ratio DRxVR
D	Diameter of film cooling hole (10mm)
R_{eD}	Reynolds number based on hole diameter
x/D	Non-dimensional streamwise distance
y/D	Non-dimensional vertical distance
z/D	Non-dimensional lateral distance
η	Local film cooling adiabatic effectiveness
$\overline{\eta}$	Laterally averaged film cooling adiabatic effectiveness ($0.0 \leq z/D < 1.5$)
η_c	Centerline film cooling adiabatic effectiveness
$\overline{\eta}_C$	Streamwise averaged centerline effectiveness
$\overline{\eta}$	Overall effectiveness (averaged over $0 \leq z/D \leq 1.5$ and over different streamwise regions)
T_∞	Mainstream temperature
T_{aw}	Adiabatic wall temperature
T_c	Coolant temperature
θ	non-dimensional temperature
Y+	Mesh dependent dimensionless distance

ACKNOWLEDGEMENT

This work is sponsored by Higher Education Commission of Pakistan under 5000 indigenous Ph.D. scholarships program.

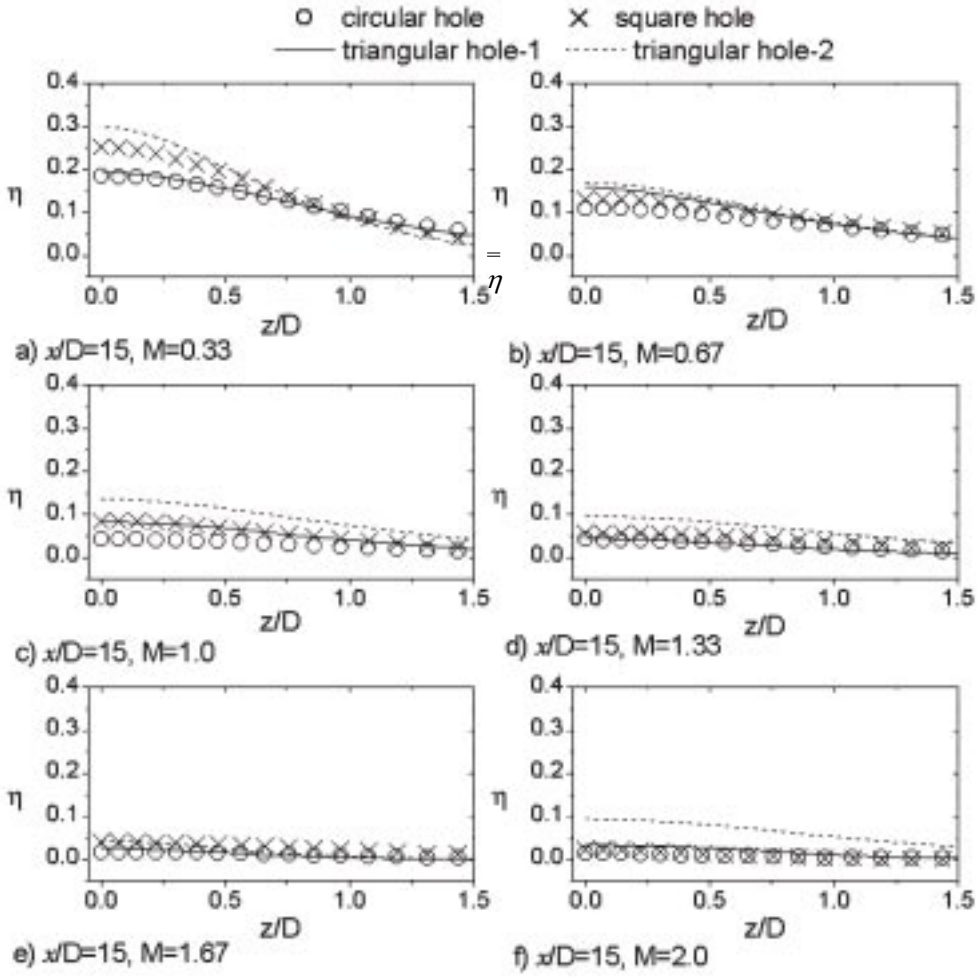

FIG. 11. LATERAL DISTRIBUTION OF EFFECTIVE AT X/D=15.0

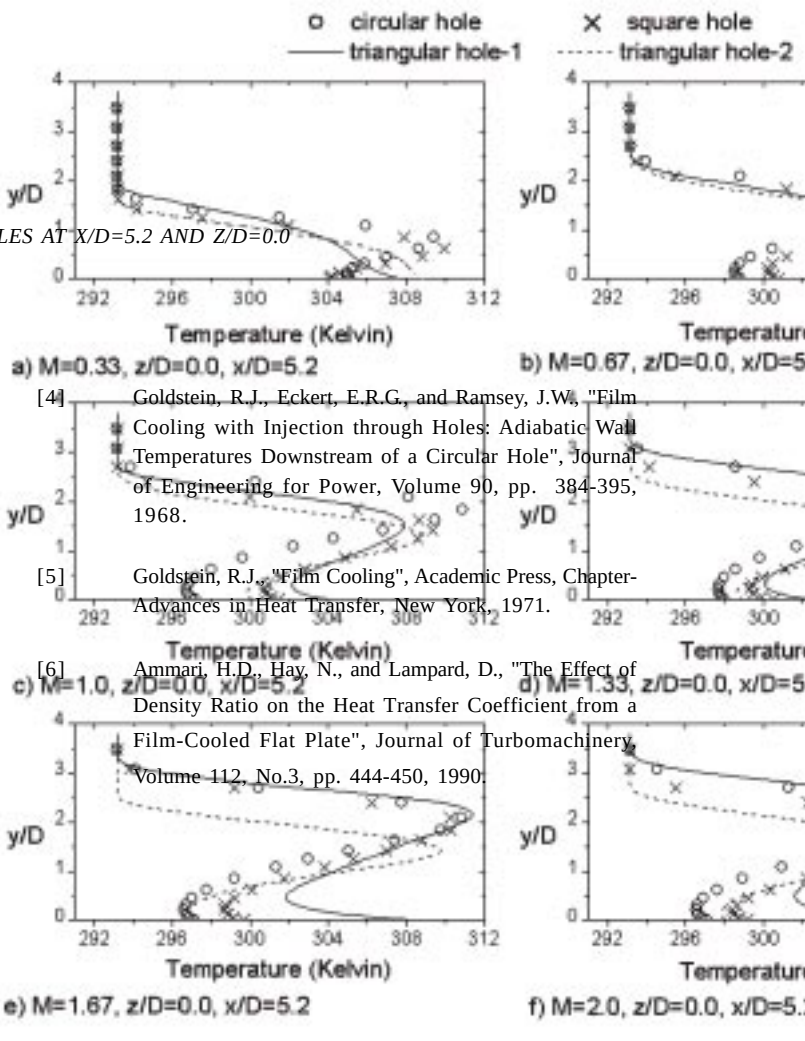

FIG. 12. TEMPERATURE PROFILES AT X/D=5.2 AND Z/D=0.0

REFERENCES

[1] Cho, H.H., and Goldstein, R.J., "Heat (Mass) Transfer and Film-Cooling Effectiveness with Injection through Discrete Holes on the Exposed Surface", Journal of Turbomachinery, Volume 117, No. 3, pp. 451-460, 1995.

[2] Forth, C.J.P., Loftus, P. J., and Jones, T. V., "Effect of Density Ratio on the Film-Cooling of a Flat Plate", AGARD Conference Proceedings, CP 390, pp. 113-143, Norway, 1985.

[3] Giang, T.T.L., "Effects of Unsteady Cooling Flow on Heat Transfer to a Film-Cooled Flat Plate", M.Sc. Thesis, Ohio State University, Columbus, 1999.

[4] Goldstein, R.J., Eckert, E.R.G., and Ramsey, J.W., "Film Cooling with Injection through Holes: Adiabatic Wall Temperatures Downstream of a Circular Hole", Journal of Engineering for Power, Volume 90, pp. 384-395, 1968.

[5] Goldstein, R.J., "Film Cooling", Academic Press, Chapter-Advances in Heat Transfer, New York, 1971.

[6] Ammari, H.D., Hay, N., and Lampard, D., "The Effect of Density Ratio on the Heat Transfer Coefficient from a Film-Cooled Flat Plate", Journal of Turbomachinery, Volume 112, No.3, pp. 444-450, 1990.

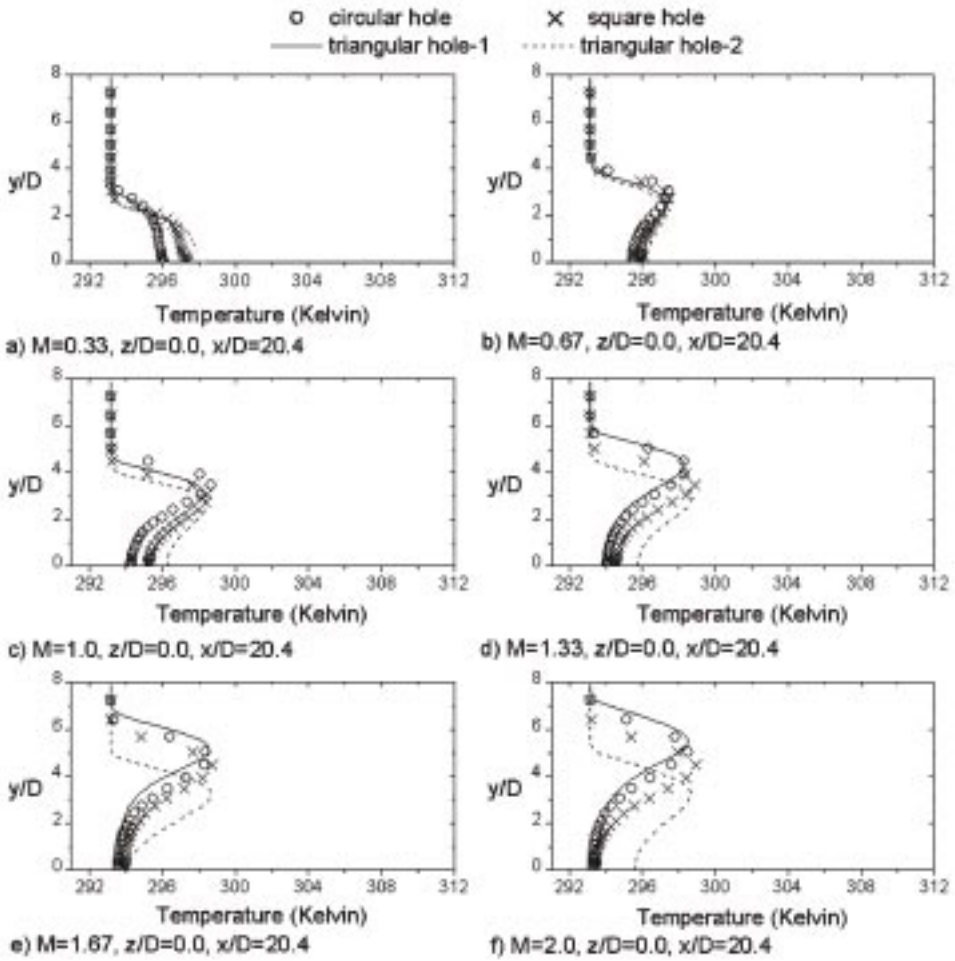

FIG. 13. TEMPERATURE PROFILES AT X/D=20.4 AND Z/D=0.0

[7] Bergeles, G. , Gosman, A.D. and Launder, B.E., "The Near Field Character of a Jet Discharged Normal to a Main Stream", Journal of Heat Transfer, Volume 98, No. 3, pp. 373-378, USA, 1976.

[8] Bergeles, G., Gosman, A.D., and Launder, B.E., "Near-Field Character of a Jet Discharged through a Wall at 30 Degrees to a Mainstream", AIAA Journal, Volume 15, No. 4, pp. 499-504, 1977.

[9] Andreopoulos, J., and Rodi, W., "Experimental Investigation of Jets in a Crossflow", Journal of Fluid Mechanics, Volume 138, pp. 92-127, 1984.

[10] Yuen, C.H.N., and Martinez-Botas, R.F., "Film Cooling Characteristics of a Single Round Hole at Various Streamwise Angles in a Crossflow: Part I Effectiveness", International Journal of Heat and Mass Transfer, Volume 46, pp. 221-235, 2003.

[11] Yuen, C.H.N., and Martinez-Botas, R.F., "Film Cooling Characteristics of Rows of Round Holes at Various Streamwise Angles in a Crossflow: Part I. Effectiveness", International Journal of Heat and Mass Transfer, Volume 48, pp. 4995-5016, 2005.

[12] Yuen, C.H.N., and Martinez-Botas, R.F., "Film Cooling Characteristics of Rows of Round Holes at Various Streamwise Angles in a Crossflow: Part II. Heat Transfer Coefficient", International. Journal of Heat and Mass Transfer, Volume 48, pp. 5017-5035, 2005.

[13] Bernsdorf, S., Rose, M.G., and Abhari, R.S., "Modeling of Film Cooling-Part I: Experimental Study of Flow Structure", Journal of Turbomachinery", Volume 128, No. 1, pp. 141-149, 2006.

[14] Ting-ting, G., and Shao-hua, L., "Numerical Simulation of Turbulent Jets with Lateral Injection into a Crossflow", Journal of Hydrodynamics, Ser.B" Volume 18, No. 3, pp. 319-323, 2006.

[15] Wang, T., and Li, X., "Mist Film Cooling Simulation at Gas Turbine Operating Conditions", International Journal of Heat and Mass Transfer, Volume 51, pp. 5305-5317, 2008.

[16] Jovanovic, M. B., Lange, H. C., and Van Steenhoven, A. A., "Effect of Hole Imperfection on Adiabatic Film Cooling Effectiveness", International Journal of Heat and Fluid Flow, Volume 29, pp. 377-386, 2008.

[17] Li, G., Zhu, H., and Fan, H., "Influence of Hole Shapes on Film Cooling Characteristics with CO2 Injection", Chinese Journal of Aeronautics, Volume 21, pp. 393-401, 2008.

[18] Launder, B. E., and Spalding, D. B., "Lectures in Mathematical Models of Turbulence", Academic Press, London, England, 1972.

[19] Launder, B. E., and Spalding, D. B., "The Numerical Computation of Turbulent Flows", Computer Methods in Applied Mechanics and Engineering, Volume 3, pp. 269-289, 1974.

[20] Barth, T. J., and Jespersen, D., "The Design and Application of Upwind Schemes on Unstructured Meshes", Technical Report AIAA-89-0366, AIAA 27th Aerospace Science Meeting, Reno, Nevada, 1989.

[21] Rhie, C. M., and Chow, W. L., "Numerical Study of the Turbulent Flow Past an Airfoil with Trailing Edge Separation", AIAA Journal, Volume 21, No. 11, pp. 1525-1532, November, 1983.

[22] Patankar, S. V., "Numerical Heat Transfer and Fluid Flow", Hemisphere Publishing Corporation, Washington, D.C., 1980.